LUND UNIVERSITY

FACULTY
OF SCIENCE

# Angular dependence of the Raman active phonon modes of Black Phosphorus

Armand Dominguez

Thesis submitted for the degree of Master of Science
Project duration: 12 months, 60 hp

Supervised by Jörgen Larsson and Åsa Bengtsson

Department of Physics
Division of Atomic Physics
May 2019

# Acronyms

IR: Infrared
BP: Black phosphorus
1D: 1 dimensional
2D: 2 dimensional
nm: nanometer
$cm^{-1}$: inverse centimeters
w.: with

# Contents

# Abstract

This Master's project presents on the angular dependence of the intensity of the Raman active phonon modes of Black Phosphorus (BP), a layered 2D material with unique and attractive characteristics to the scientific and engineering community. Raman spectroscopy is an indispensable tool in quick and unobtrusive analysis of chemical structures.

In this Master project, the structure of BP is analyzed through polarized Raman excitation. The incident polarization is varied to investigate the effect on the various detectable Raman active modes in BP. A Raman microscope with a 532 nm laser was used to excite BP flakes mechanically exfoliated from a source. The amplitude of the peaks in the Raman spectra are plotted against the angle that they were measured in. The classical model for the Raman tensor was used but it was inadequate in it's ability to predict data in the cross polarized configuration. An improved model taking the linear dichroism and the degradation effects of BP into account substantially improved the fit.

All in all, with the strange characteristics of BP factored, the complex angular dependence set by theory predicts most of the experimental angular dependence, however certain Raman modes do not fit the model as well as others.

# Acknowledgements

I would like to thank my supervisor, Prof. Jörgen Larsson for his solid advice, patience and good humour over the course of this project. I would also like to thank Åsa Bengtsson, Xiaocui Wang and Carl Ekström for the additional help in both the lab and the office.

Finally, I would like to thank my family for giving me the opportunity to pursue this program in the first place.

# Popular Science

Once in a while, a new material emerges with unique characteristics that make it of particular interest to many. Black Phosphorus (BP) may be one of those peculiar materials.

BP is made of many sheets; like stacks of paper. It is possible to keep peeling off the sheets of BP until one only has a single sheet left. Doing so reveals BP's interesting properties. When it becomes several sheets thin it acts like a semiconductor; one of the necessary parts of a computer chip. If the semiconductor part of a computer chip is small then the overall size of the computer chip can be even smaller, and if the computer chip is smaller then the same device can be made more compact or more powerful for the same size.

A problem when working with these thin materials is that it is difficult to determine the orientation of the material which can be important in some applications. Many methods can determine the orientation of the material but can damage the item when done. However, there exists a method called Raman spectroscopy which uses the fact that sometimes light does not bounce back the same way when it hits an object. Sometimes the light that bounces off the object is a different color. The amount of light that is a different color depends on the object that one is shining light on. In the case of BP, this also depends on the angle you shine the light on. Because of this, one can map the orientation of BP using Raman spectroscopy, the technique used in this project.

# 1 Introduction

The advent of graphene has created a great interest in 2D materials and their interesting characteristics. One in particular is called black phosphorus(BP) [1]. Although first discovered in 1914, it was not until 2014, with the ongoing mass excitement over 2D materials, that BP was studied intensely.

The unique characteristics of BP make it a material of scientific inquiry [2]. One such characteristic is that BP has a tunable bandgap [2–4]; thus making it a potential material for semiconductors [5]. Unfortunately, BP degrades in normal environments making it difficult to mass produce and use [6]. Further studies need to be made into BP from an electrical and optical perspective to be able to create practical applications from BP.

Raman spectroscopy is a non-invasive and low-damaging method for analyzing materials [7]. Raman spectra say much about the structure of a material and whatever defects it might have if the material is Raman active [8]. Therefore, it makes a prime method for studying BP without greatly damaging the substance [4, 9, 10].

The aim of this project is to investigate the angular dependence of the intensity of the phonon modes of BP. By controlling the polarization of the incoming light, information regarding the angular dependence of BP can be used to determine the orientation of the BP sample for use in further applications [11–14].

# 2 Theory

## 2.1 Phonons

Phonons are the collective excitation of particles set in a periodic and elastic arrangement in condensed matter. A phonon is defined as a quasiparticle and it describes the vibrational modes of freedom in a lattice.

The classical description of phonons involves modelling them as harmonic oscillators. From Newton's law we have:

$$F = ma = m\frac{d^2x}{dt^2} = -cx \tag{1}$$

where the product of mass and acceleration is equal to the product of c, the spring constant and x, the displacement from equilibrium.

The most basic environment of a phonon would be in a 1D system of connected harmonic oscillators where the particles are balls and the intermolecular forces are modelled as springs as seen in figure 1.

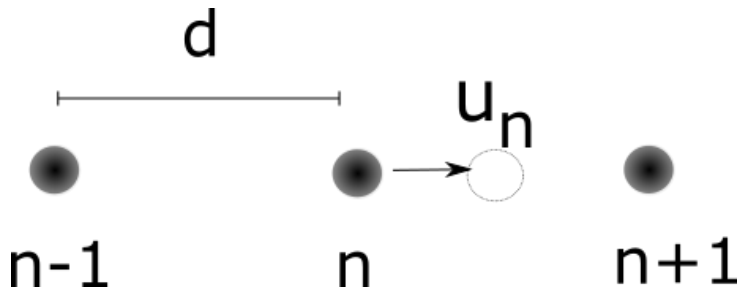


Figure 1: An example of a simple 1D system

Let there be an nth particle in the system where the particle to the right is n+1, the particle to the left is n-1, the distance between particles is d and the displacement of each particle is $u_n$ denotes which particle the displacement belongs to. Since the force acting on a harmonic oscillator is equal to the product of the springs constant (c) and the displacement then, a coupled equation including the displacements of the surrounding particles can be made to describe the motion of particle n.

$$c(-2u_n + u_{n-1} + u_{n+1}) = m\frac{du^2}{dt^2} = F \tag{2}$$

Using the trial solution to

$$u_n = Ae^{i(cnd-\omega t)} \tag{3}$$

to get

$$M(-\omega^2)e^{iknd} = -c(2e^{iknd} - e^{ik(n+1)d} - e^{ik(n-1)d}) \tag{4}$$

Solving for $\omega$ leads to the dispersion relation of:

$$\omega(k) = 2\sqrt{\frac{c}{M}}sin(\frac{kd}{2}) \tag{5}$$

The dispersion relation shows the effect that dispersion will have on a wave travelling through the medium as a function of the wavenumber k in this particular case.

Although the basic 1D chain is useful in showing the concept of a phonon, it does not account the effect of noncoherent movement in the lattice. A linear diatomic chain is a more complicated but much more useful model for explaining the concepts in this Master thesis. Instead of a chain consisting of only one type of atom as in figure 1, the chain now consists of 2 types of atoms of different masses ($M_1 < M_2$)alternating between each other along the chain as in figure 2.

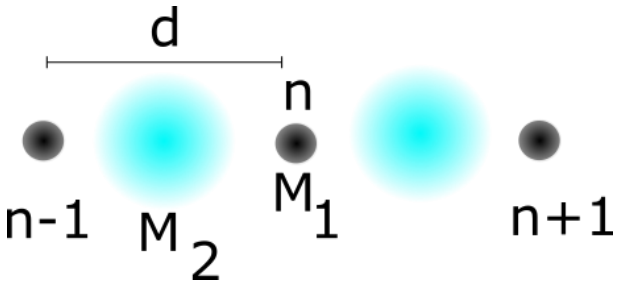


Figure 2: A static linear diatomic chain

After following through a similar process to the simple one dimensional chain, the dispersion relation is:

$$\omega^2 = C\left(\frac{1}{M_1} + \frac{1}{M_2}\right) + C\sqrt{\left(\frac{1}{M_1} + \frac{1}{M_2}\right)^2 - \frac{4sin^2(kd/2)}{M_1 M_2}} \tag{6}$$

The additional particle type allows a separate movement to occur showing mathematically as two different roots. The existence of two roots leads to the conclusion that there are two types of phonons. The positive root is the optical phonon while the negative root is the acoustic phonon.

A dispersion curve can be seen in figure 3 where $\frac{\pi}{a}$ and $-\frac{\pi}{a}$ are the boundaries of the Brillouin zone, which is the unit cell of a reciprocal lattice[1]. In figure 3, the optical phonons have a higher dispersion than the acoustic phonons.

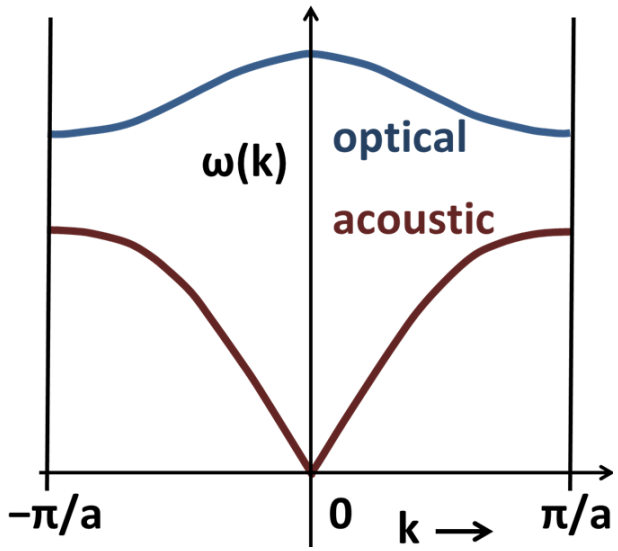


Figure 3: Dispersion curves for the acoustic and optical phonons of a linear diatomic chain (From https://en.wikipedia.org/wiki/Diffractiongrating/media/File : DiffractionGratingEquation.jpg)

[1]The Fourier transform of another lattice

An example of the respective movements of the two phonons can be seen in figure 4. Acoustic phonons are coherent movements of the particles; the particles move in the same direction together. Conversely, optical phonons exist when adjacent particles have incoherent movement, i.e. they do not move in the same direction. Although BP consists of multiple phosphorus atoms, it is possible to achieve both optical and acoustic phonons in 3D due to the additional degrees of freedom.

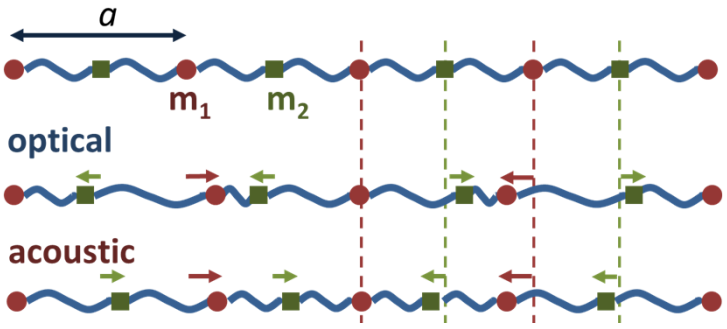


Figure 4: An example of a simple linear diatomic chain in motion.

Since this Master's project relies on Raman scattering, this thesis will focus on the the detectable optical phonons of BP that can be controlled through polarized Raman excitation.

## 2.2 Fundamentals of Group theory

In Mathematics, groups are collections of objects that can combine with each other to form another object whilst following these four axioms [15–18].

1. All elements of a group G can be associated with another element within G. This operation is well known as multiplication and the product is still part of the group
2. Multiplication is associative. For example, (XY)Z=X(YZ)
3. There is an identity element that allows an element to be equal to itself when multiplied to the identity element. This is identical to multiplying by 1.
4. There is an inverse element to all elements. Multiplying an element by its inverse results in the identity element.

Space groups are groups that follow the 4 axioms of Group theory and retain the overall symmetry of the crystal. Unit cells are what make up the space groups. In the case of spectroscopy the entire space group is not necessary as it also contains translation. Instead, it is sometimes more practical to use point groups since these contain the symmetry or general structure of the molecular system.

Point groups are symmetric groups that keep at least one point fixed. There are infinite many point groups but they can be classified into several types. For this Master's thesis, Schoenflies notation is used. In the Schoenflies notation the letter represents the classification or family of the group, while the subscript denotes any additional symmetry attributes. Occasionally, superscripts may be included for additional classification of space groups but it gives no additional information on hand without looking at the character table[2] for the point group.

[2] A character table shows the irreducible group representations and conjugacy classes of a given point group.

## 2.3 Black Phosphorus

The $D_{2h}^7$ point group [19] for BP represents a puckered honey comb or orthorhombic structure. The structure of BP can be derived from the more symmetric graphite which is described by the point group $D_{6h}^1$. Both fall under the general point group, of $D_{nh}$ where D means that the structure is two sided and has n fold rotation axis and n twofold axes perpendicular to that axis with an additional horizontal mirror plane. By uniaxially compressing the $D_{6h}^1$ as seen in figure 5, results in the $D_{2h}^{19}$ subgroup [15]. This subgroup no longer retains its hexagonal symmetry. As a possible consequence, the newly orthorhombic structure may displace atoms in periodic structure up and down the z direction perpendicular to the strain. This new zig zag structure is under the $D_{7h}^2$ group that BP falls under.

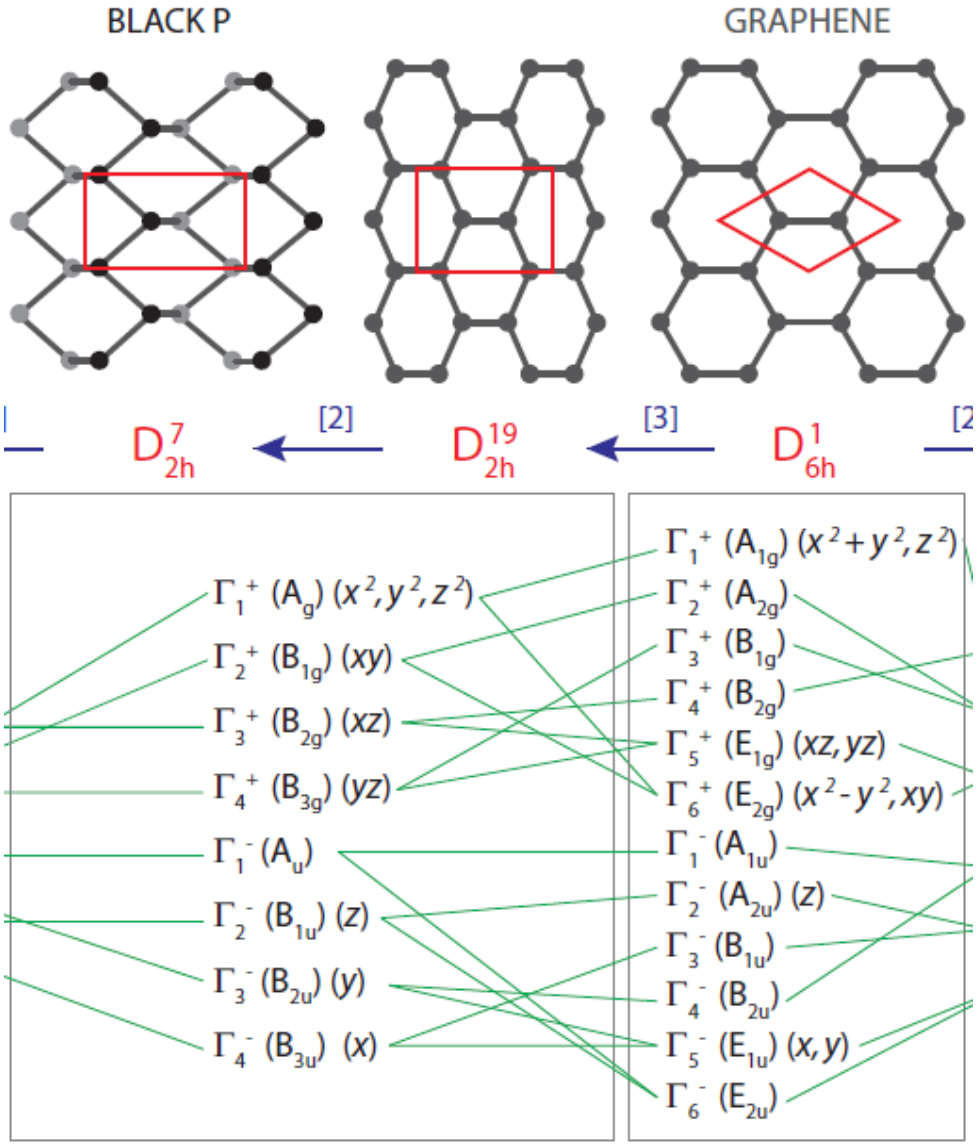


Figure 5: $D_{6h}^1$ space group transformed to the $D_{2h}^7$ space group. The table below contains the modes of both groups [15]

The character table for the $D_{2h}^7$ point group is shown in figure 6. For this Master's project, the most important parts of this character table are the first and last columns. The conjugacy tells about the symmetry of the mode, while the quadratic column shows if the mode is Raman active(will be explained in section 2.6). From the character table (2.2) the modes $A_g$, $B_{1g}$, $B_{2g}$. and $B_{3g}$ are Raman active because their irreducible representations transform as quadratic basis functions. i.e. the transformation equals one of these forms: $x^2$,$y^2$,$z^2$,$xy$,$xz$,$yz$. [15]

| $D_{2h}$ ($mmm$) | $E$ | $C_2(z)$ | $C_2(y)$ | $C_2(x)$ | $i$ | $\sigma(xy)$ | $\sigma(xz)$ | $\sigma(yz)$ | | |
|---|---|---|---|---|---|---|---|---|---|---|
| $A_g$ | 1 | 1 | 1 | 1 | 1 | 1 | 1 | 1 | | $x^2, y^2, z^2$ |
| $B_{1g}$ | 1 | 1 | −1 | −1 | 1 | 1 | −1 | −1 | $R_z$ | $xy$ |
| $B_{2g}$ | 1 | −1 | 1 | −1 | 1 | −1 | 1 | −1 | $R_y$ | $xz$ |
| $B_{3g}$ | 1 | −1 | −1 | 1 | 1 | −1 | −1 | 1 | $R_x$ | $yz$ |
| $A_u$ | 1 | 1 | 1 | 1 | −1 | −1 | −1 | −1 | | |
| $B_{1u}$ | 1 | 1 | −1 | −1 | −1 | −1 | 1 | 1 | $z$ | |
| $B_{2u}$ | 1 | −1 | 1 | −1 | −1 | 1 | −1 | 1 | $y$ | |
| $B_{3u}$ | 1 | −1 | −1 | 1 | −1 | 1 | 1 | −1 | $x$ | |

Figure 6: Character table for the $D_{2h}$ point group. The right most column shows the transformation of the basis function. [20]

Figure 7 shows the five atomic displacements of the Raman active modes. This view is from the armchair view or the side view of the BP flake. The $A_g^1$ mode moves in the y direction, while the $A_g^2$ mode moves in the x direction. The $B_{1g}$ and $B_{2g}$ modes have movement in the z direction while both $B_{3g}$ modes have movement in the x direction.

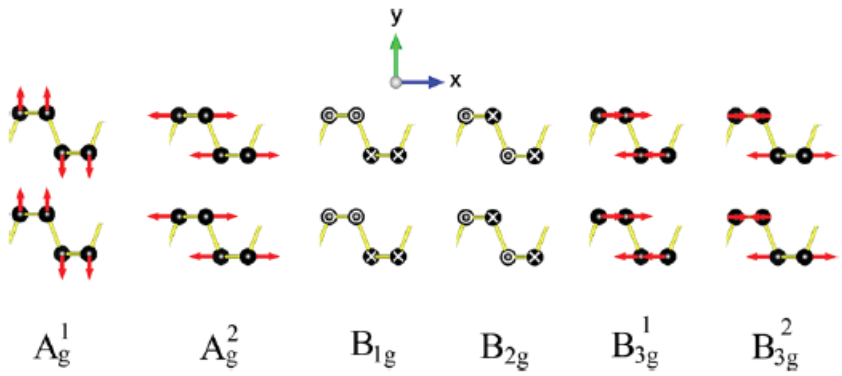


Figure 7: The valid Raman modes of BP [28]

### 2.3.1 Degradation

Scientific studies have shown that BP degrades in exposure to light and oxygen [21, 22]. Although research is still ongoing regarding the exact process of BP degradation, common results point to a chemical reaction that occurs on the exposed surfaces of BP. The degradation causes increased lattice spacing and oxidation, eventually leading to the formation of oxides [22]. Furthermore, when water reacts to oxidized BP, phosphoric acid forms on the surface which accelerates degradation further.

Alsaffar *et al.* [21] report that the Raman intensity of the BP modes initially increase during the first 15 days but decrease quickly afterwards and that the speed of degradation is inversely proportional to the thickness

## 2.4 Fundamentals of light

From classical electromagnetism, we know that Maxwell's equation are [23]:

$$\begin{aligned} \nabla \cdot \vec{E} &= \frac{\rho}{\epsilon} \\ \nabla \cdot \vec{B} &= 0 \\ \nabla \times \vec{E} &= -\frac{d\vec{B}}{dt} \\ \nabla \times \vec{B} &= \mu\Big(\vec{J} + \epsilon\frac{d\vec{E}}{dt}\Big) \end{aligned} \tag{7}$$

where $\vec{E}$ is the electric field, $\vec{B}$ is the magnetic field, $t$ is time, $\vec{J}$ is the electric current density, $\epsilon$ is the permittivity of free space and $\mu$ is the permeability of free space.

If one assumes a vacuum with no free charges, it is possible to derive the wave equations in a vacuum from Maxwell's equations (See derivation):

$$\begin{aligned} \frac{1}{c^2}\frac{\partial^2\vec{E}}{dt^2} - \nabla^2\vec{E} = 0 \\ \frac{1}{c^2}\frac{\partial^2\vec{B}}{dt^2} - \nabla^2\vec{B} = 0 \end{aligned} \tag{8}$$

where $c$ is the speed of light in a vacuum.

A solution to the wave equation is a plane wave :

$$\vec{E} = \vec{E_0}cos(\vec{k}\cdot\vec{r} - \omega t + \phi) \tag{9}$$

where $\vec{E_0}$ is the amplitude of the electric field, $\vec{k}$ is the wave vector, $\vec{r}$ is the position vector, $\omega$ is the angular frequency of the electric field and $\phi$ is the initial phase of the wave. In three dimensions, it can be seen that $\vec{E}$, $\vec{B}$ and $\vec{k}$ are all orthogonal to one another. Therefore, the electric field, and the magnetic field are both oscillating perpendicularly to the direction of propagation.

If one assumes that the electric field is oscillating in the x direction, and the magnetic field is oscillating in the y direction, one can rewrite the equation as:

$$\vec{E}_x(z,t) = \vec{E_0}cos(kz - \omega t + \phi) \tag{10}$$

## 2.5 Polarization

Polarization describes the direction of the oscillations of light [24].Generally, light is elliptically polarized. Since equation 10 can be represented as the sum of two orthogonal vectors, one can separate the amplitude of the x and y components into

$$\vec{E_{0x}}(z,t) = E_{0x}cos(\omega t - kz + \phi_x)\hat{e}_x \tag{11}$$

$$\vec{E_{0y}}(z,t) = E_{0y}cos(\omega t - kz + \phi_y)\hat{e}_y \tag{12}$$

where $E_{0x}$ and $E_{0y}$ are the amplitudes of the electric field in in their respective planes, and $\phi_x$ and $\phi_y$ are the phases of the fields. [25]

Linearly polarized light will be used it allows a controlled method of measuring the angular dependence of the Raman active modes of BP. The equation of light that will be used for controlling the polarization of the light will be the normalized Jones matrix[3] formulation for vertically polarized light:

$$\begin{pmatrix} 0 & 0 \\ 0 & 1 \end{pmatrix} \tag{13}$$

## 2.6 Scattering: A classical depiction

Scattering is a phenomenon that can occur when light interacts with matter. Scattering can be explained by modelling a molecule as a simple harmonic oscillator. The oscillating electromagnetic field of light will interact with the electrical system of the molecule. This interaction will induce a dipole moment. The dipole moments induced by the light creates a macroscopic polarization that acts as a secondary electric field. This secondary electric field is scattered light.

$$\vec{p} = \alpha\vec{E} \tag{14}$$

The classical description for scattering begins with an equation describing the induced dipole moment. In equation 14, p is the induced dipole moment caused by the electric field $\vec{E}$, and $\alpha$ is the polarizability of the molecule [26]. The polarizability of a molecule reflects it's tendency to be distorted by and external electric field.

The polarizability can be estimated by Taylor expanding $\alpha$ around the geometry of the nucleus leading to the equation:

$$\alpha = \alpha(Q) = \alpha_0 + \sum_{q=1}^{N}\left((q\frac{\partial\alpha}{\partial q})_{qo} + (qq'\frac{\partial^2\alpha}{2\partial q\partial q'}) + \mathcal{O}(q^3)\right) \tag{15}$$

where q are individual normal modes, $q_0$ is the equilibrium nuclear geometry and $N$ is the number of all normal modes $q$.

[3]Jones matrices are operators that act on the equations of light when they are expressed as a vector. [27]

We can define these normal modes $q$ as a simple harmonic oscillator:

$$q = q_0 cos(\omega_q t) \tag{16}$$

where $\omega_q$ represents the oscillations with a characteristic frequency at q. By combining equations 15, 16 through inserting 16 into 15 and further truncating the equation we get:

$$\alpha = \alpha(Q) = \alpha_0 + \sum_{q=1}^{N} \left( \left( q \frac{\partial \alpha}{\partial q} \right)_{qo} q_0 cos(\omega_q t) \right) \tag{17}$$

Finally by substituting equation 17 into 14, and recalling that the dipole moment is induced by the external electric field with oscillation $\omega_0$:

$$\vec{E} = \vec{E_0} cos(\omega_0 t)$$

We have:

$$\vec{p} = \alpha(Q)\vec{E} = \left( \alpha_0 + \sum_{q=1}^{N} \left( \left( q \frac{\partial \alpha}{\partial q} \right)_{qo} q_0 cos(\omega_q t) \right) \right) \vec{E_0} cos(\omega_0 t) \tag{18}$$

One can further dissect this equation into different sources of scattering by using a trigonometric formula for cosine products to get:

$$\begin{aligned} \vec{p} = {} & \alpha_0 \vec{E_0} cos(\omega_0 t) \\ & + \frac{1}{2} \left( \frac{\partial \alpha}{\partial q} \right)_{q0} \vec{E_0} q_0 cos(\omega_0 t - \omega_q t) \\ & + \frac{1}{2} \left( \frac{\partial \alpha}{\partial q} \right)_{q0} \vec{E_0} q_0 cos(\omega_0 t + \omega_q t) \end{aligned} \tag{19}$$

The first term in equation 19 is the well known and studied Raleigh scattering. As can be seen in the equation, this particular term shares the same frequency as the external light. Since this term has no change in frequency, it is considered an elastic process where the initial energy is conserved.

The second term in the equation represents a decreased frequency from the original source. This red-shifted term with respect to the original excitation frequency is the source of the Stokes scattering term.

The third term in equation 19 is a higher frequency term and it represents the source of anti-Stokes scattering.Anti-stokes scattering results in blue-shifted light. A Jablonski diagram depicts the differences in energy levels from the Raman and Raleigh shifts (Figure 8). As can be seen by the thickness of the arrows, the Rayleigh scattering has the greatest intensity, while the anti-stokes Raman scattering has the least.

Of these three terms, this Master project will focus on Stokes scattering since Raleigh scattering does not contain data regarding the molecular degrees of freedom and anti-Stokes scattering has a significantly lower intensity in comparison to the Stokes scattering making it more difficult to detect. The Raman shift resulting from the Stokes scattering is

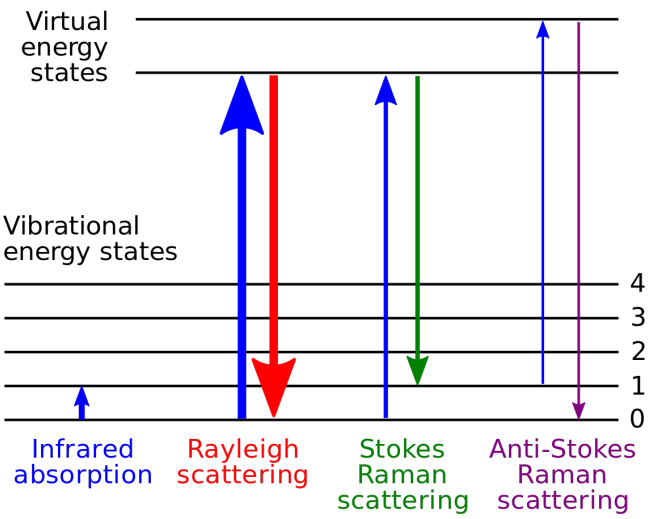


Figure 8: Jablonski diagram of the different scattering types

measured in wavenumbers with inverse centimeters ($cm^{-1}$) as the unit [7] . The conversion for inverse centimeters to nanometers is as follows:

$$\delta\nu(\mathrm{cm}^{-}1) = \left(\frac{1}{\lambda_0(\mathrm{nm})} - \frac{1}{\lambda_1(nm)}\right) \times \frac{10^7\,\mathrm{nm}}{\mathrm{cm}} \tag{20}$$

where $\lambda_0$ is the original wavelength of the light and $\lambda_1$ is the new wavelength of the shifted light.

## 2.7 Raman selection rule

Unlike Raleigh scattering which is dependent on the polarizability of a molecule at its equilibrium position, Raman scattering requires the molecular polarizability of possible states to be different.This require the polarizability to change with respect to the coordinate of the vibration. Therefore, one can make a generalization that the material is Raman active if $\frac{\partial\alpha}{\partial q} \neq 0$.

Additionally, as laid out in Appendix D3 of [15], modes are only Raman active if their irreducible representations transform as quadratic basis functions and their combinations ($x^2$,$y^2$,$z^2$,$xy$,$xz$,$yz$).

The setup in the experiment is in a backscattering geometry. In this setup, the incident light strikes the hexagonal plane of the sample (not the zigzag side view). Of the Raman active modes, only the $A_g^1$, $B_{2g}$ and $A_g^2$ modes can be detected due to the direction of that they oscillate in.

## 2.8 Raman tensor

The intensity of the Raman scattering is given by the Raman cross section [28]:

$$S_k \propto \left| \hat{e_i} \cdot R_k \cdot \hat{e_s} \right|^2 \tag{21}$$

where the incident light is

$$\hat{e_i} = (sin\theta \quad 0 \quad cos\theta) \tag{22}$$

the scattered light is

$$\hat{e_s} = (sin\theta \quad 0 \quad cos\theta) \tag{23}$$

in the parallel configuration, while it is

$$\hat{e_s} = (cos\theta \quad 0 \quad -sin\theta) \tag{24}$$

in the cross configuration. These configurations are the relationship between the polarizer and the incoming laser light. $\theta$ is the angle of the polarization of the laser with respect to the orientation of the surface of the sample. Since the orientation of the sample is unknown, a coordinate system can only be found by fitting the general angular dependence of the intensity with experimental data [14]. The parallel configuration allows the same polarization of light as the incident light to pass through while the cross configuration allows light perpendicular to the incident light to pass. Finally $R_k$ is the Raman tensor, which may take a different form depending on the mode in question [28]:

For the $A_g$ modes, the Raman tensor has the form:

$$\begin{vmatrix} a & 0 & 0 \\ 0 & b & 0 \\ 0 & 0 & c \end{vmatrix}$$

For the $B_{1g}$ the form is:

$$\begin{vmatrix} 0 & d & 0 \\ d & 0 & 0 \\ 0 & 0 & 0 \end{vmatrix}$$

The $B_{2g}$ is:

$$\begin{vmatrix} 0 & 0 & f \\ 0 & 0 & 0 \\ f & 0 & 0 \end{vmatrix}$$

and the $B_{3g}$ mode has the form:

$$\begin{vmatrix} 0 & 0 & 0 \\ 0 & 0 & g \\ 0 & g & 0 \end{vmatrix}$$

Of these modes, only the $A_g$, $B_{2g}$ will be seen with the backscattering setup used in this experiment. Specifically, there will be 3 modes that will be seen using Raman spectroscopy: $A_g^1$, $A_g^2$, and $B_{2g}$. Using this knowledge, the expressions for the angular dependencies of the 3 modes can be be obtained by inserting equations 22, 23 (or 24 if in the cross polarized configuration) and the appropriate $R^k$ into equation 21:

$$S_{A_g \text{ parallel}} = (a\, sin^2\theta \ + c\, cos^2\theta)^2 \tag{25}$$

$$S_{A_g \text{ cross}} = ((a-c)\, cos\theta\ sin\theta)^2 \tag{26}$$

$$S_{B_{2g} \text{ parallel}} = (2\, f\, cos\theta\, sin\theta)^2 \tag{27}$$

$$S_{B_{2g} \text{ cross}} = (f\, cos(2\theta))^2 \tag{28}$$

According to Ribereiro *et al.* [28], the derived expressions are inadequate for explaining the angular dependence of BP. Ribereiro *et al.* claims that due to the linear dichroism[4] found in BP, the light absorption must be taken into account in the Raman tensor elements. This is done by using the complex nature of the dielectric function of absorptive materials and redefining the Raman tensor element to $R_{ij}^k$.

The $R_{ij}^k$ element of the Raman tensor is dependent on the derivative of the dielectric function with respect to the normal coordinate. Since the dielectric function, $\epsilon_{ij} = \epsilon'_{ij} + i\epsilon'_{ij}$, $R_{ij}^k$ must also be a complex value:

$$R_{ij}^k = \frac{\partial \epsilon_{ij}}{\partial q^k} = \frac{\epsilon'_{ij}}{\partial q^k} + i\frac{\partial \epsilon''_{ij}}{\partial q^k} \tag{29}$$

One can rewrite the Raman tensor elements as complex functions:

$$a = ae^{i\phi_a} \tag{30}$$

$$c = ce^{i\phi_c} \tag{31}$$

$$d = de^{i\phi_d} \tag{32}$$

where $\phi_{a,c,d}$ are the phases of the respective tensor elements that are being studied in the backscattering setup. These tensor phases are defined as:

$$\phi_a = \arctan\frac{\frac{\partial \epsilon''_{xx}}{\partial q^{A_g}}}{\frac{\partial \epsilon'_{xx}}{\partial q^{A_g}}} \tag{33}$$

[4]Linear dichroism is a property of a material where the absorption of light is polarization dependent.

$$\phi_c = \arctan\frac{\frac{\partial \epsilon''_{zz}}{\partial q^{A_g}}}{\frac{\partial \epsilon'_{zz}}{\partial q^{A_g}}} \tag{34}$$

$$\phi_d = \arctan\frac{\frac{\partial \epsilon''_{xz}}{\partial q^{B_{2g}}}}{\frac{\partial \epsilon'_{xz}}{\partial q^{B_{2g}}}} \tag{35}$$

As with the simpler expressions, we use the vectors of the incoming and scattered light to determine the angular dependency of the modes to get:

$$S_{A_g \text{ parallel}} = (asin^2\theta + ccos\phi_{ca}cos\ 2\theta)^2 + c^2sin^2\phi_{ca}cos^4\theta \tag{36}$$

$$S_{A_g \text{ cross}} = ((a - ccos\phi_{ca})^2 + c^2sin^2\phi_{ca})sin^2\theta cos^2\theta \tag{37}$$

$$S_{B_{2g} \text{ parallel}} = (2dsin\theta cos\theta)^2 \tag{38}$$

$$S_{B_{2g} \text{ cross}} = (dcos2\theta)^2 \tag{39}$$

Equations 36 and 37 incorporate the new phase shift of the phases of the Raman tensor while equations, 38 and 39 retain the same formulas as equations 27 and 28 due to the cancellation of $\phi_d$ in when taking the absolute value of the complex phase.

# 3 Experiment

## 3.1 Confocal Raman Spectroscopy

Raman spectroscopy is a method of detecting and analyzing the Raman effect. Like other spectroscopic methods, Raman spectroscopy involves separating incident light into its component wavelengths using a grating and utilizing a CMOS to analyze the spectrum.

The particular setup used in the experiment consists for a reflective grating and two curved mirrors as can be seen in figure 9. The setup is in a back scattering geometry. The incoming 532 nm laser light is sent towards the sample from tube 1 in figure 10.

After the light strikes the sample and the back-scattered light is reflected into tube 2 where it propagates toward the entrance slit in figure 9.

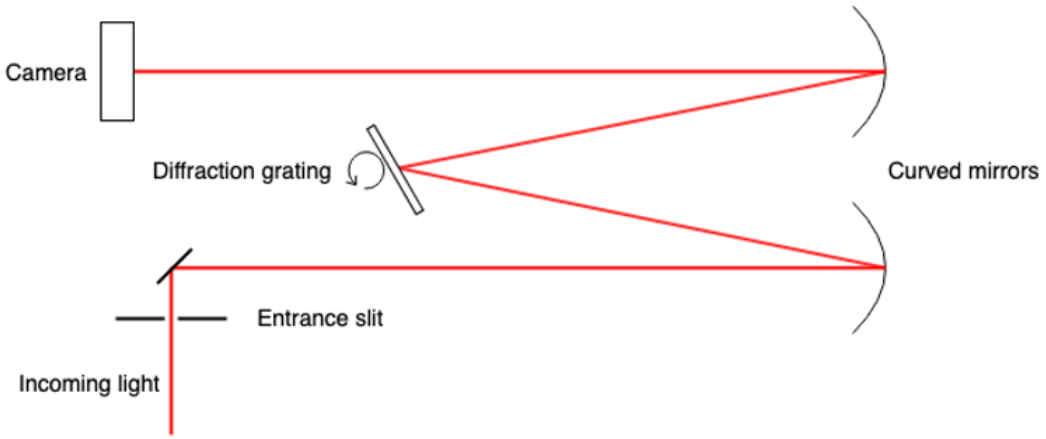


Figure 9: A basic schematic of the Raman spectrometer in use [29]

After passing through the entrance slit, the light is collimated by mirror 1 onto the diffraction grating as seen in 9. There are three choices of gratings in this particular system: 150g, 300g 1200g. These numbers represent the density of grooves per mm length of the grating. The light follows the grating equation of:

$$sin\theta_q = -sin\theta_i + \frac{q\lambda}{\Lambda} \tag{40}$$

where q is the order of the light, $\lambda$ is the wavelength of the light, $\Lambda$ is the distance between grooves and $\theta_i$ is the incoming light. From equation 40, it is known that longer wavelengths are deflected at a greater angle. Afterwards, the light is refocused by the second curved mirror onto the Andor Zyla CMOS camera.

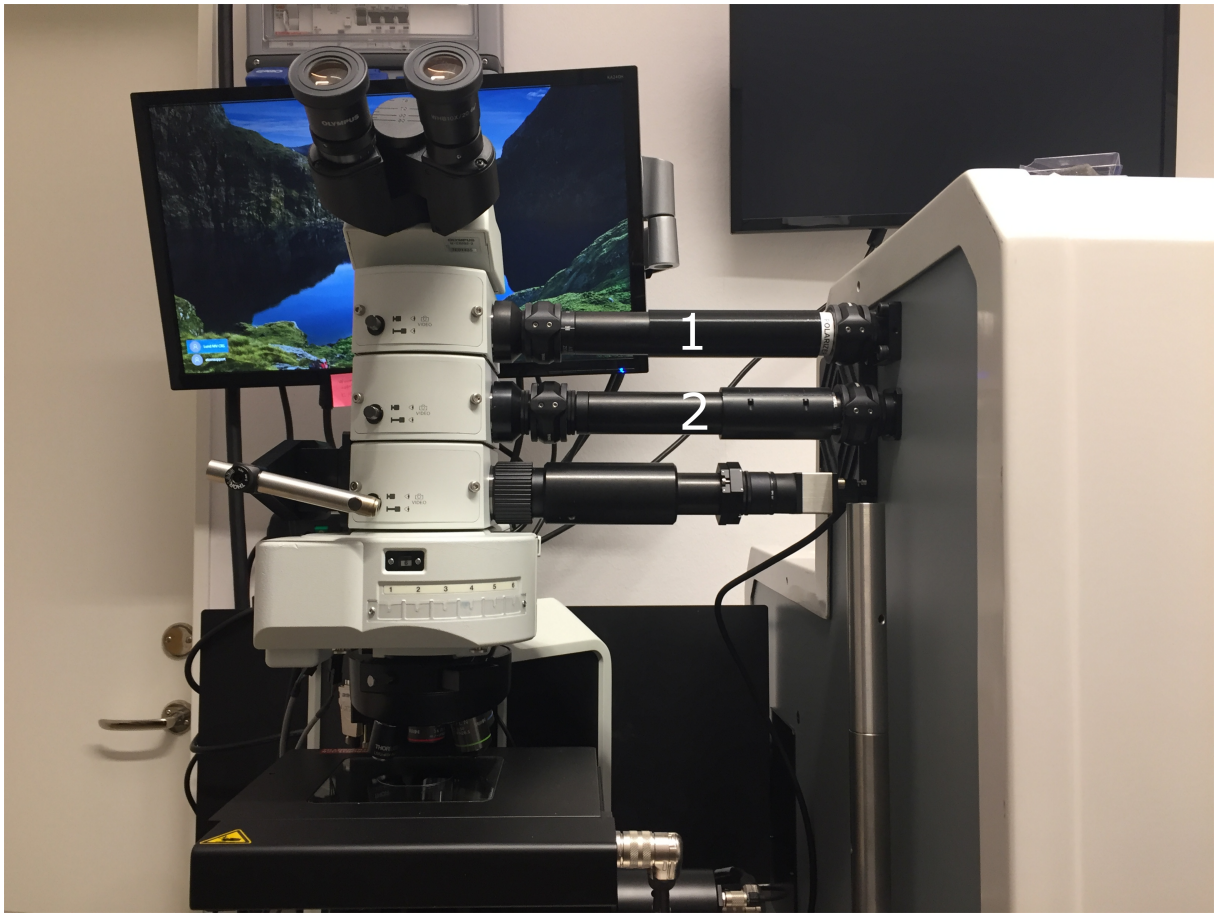


Figure 10: Photo of the exposed section of the Raman microscope. Tube 1 is the incoming light, and tube 2 has the scattered light

## 3.2 Implementing Phonon mode control

Phonon mode control is achieved via the rotation of the polarized laser light. In order to achieve proper excitation and detection of the phonons, 4 additional optical components have been added to the setup as seen in figure 11. Each component was mounted on a rotator mount.

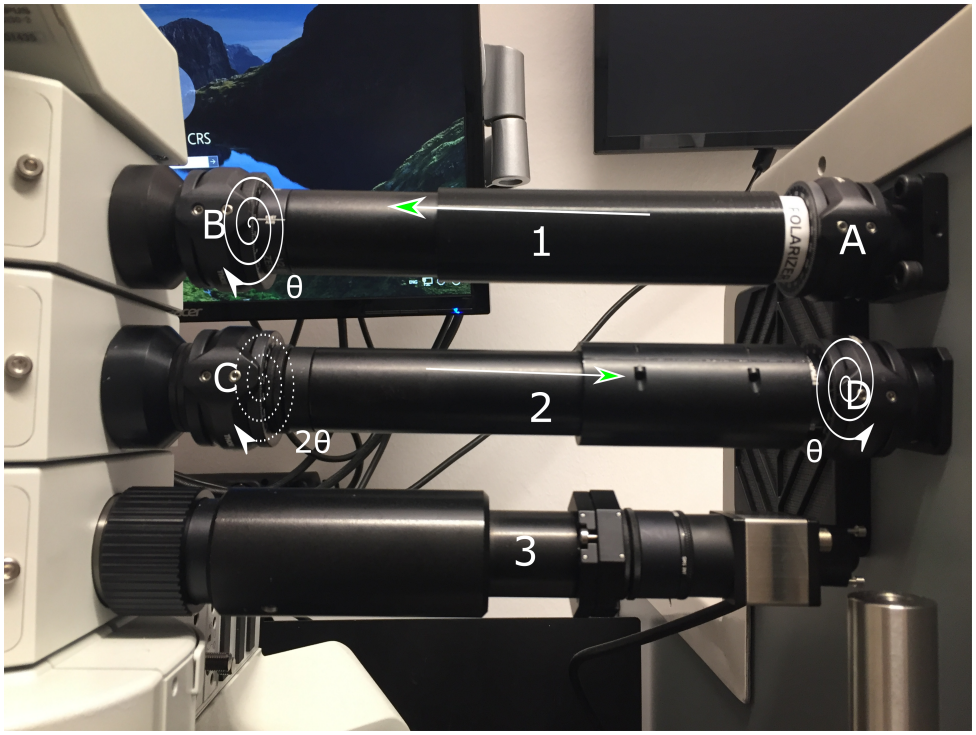


Figure 11: Photo of the optics added for phonon mode control with labels

The first optical component(A) the laser passes through is a Thorlabs economy film polarizer for 532 nm light. This is in place to ensure that the incoming laser light is properly polarized. This optical component does not rotate and the light is vertically polarized. The Jones matrix for this polarizer is:

$$\begin{pmatrix} 0 & 0 \\ 0 & 1 \end{pmatrix} \tag{41}$$

After the polarizer, the laser passes through component B,quartz zero order waveplate from Thorlabs. This half-wave plate is the main method of phonon mode control as it is what rotates the polarization of the laser before the laser hits the sample. A waveplate does this by shifting the phase of the perpendicular polarizations of the incoming light through birefringence. In Jones matrix form this waveplate can be expressed as:

$$e^{\frac{-i\pi}{2}} \begin{pmatrix} cos^2\theta - sin^2\theta & 2cos\theta sin\theta \\ 2cos\theta sin\theta & sin^2\theta + icos^2\theta \end{pmatrix} \tag{42}$$

When combined with 13, this effectively results in a $2\theta$ rotation where $\theta$ is the angle that the waveplate has been rotated.

Upon reaching the sample, the light is backscattered through component C, a polarizer. This component is rotated by an angle $2\theta$ where $\theta$ is the angle that the waveplate is rotated. This polarizer controls which phonon modes are being detected as well as whether or not the setup is parallel or cross polarized. The Jones matrix for this polarizer is:

$$\begin{pmatrix} sin\theta & 0 \\ 0 & cos\theta \end{pmatrix} \tag{43}$$

The last optical component the light passes through is another identical waveplate to the one previously used. The purpose of this waveplate is to maximize the efficiency of the spectrometer. It was experimentally determined that the spectrometer is most efficient when the incoming laser light is horizontally polarized. Ergo, this waveplate is set to guarantee that the polarization of the light passing through the entrance slit is horizontally polarized.

Careful attention was given to the potential beam deviation caused by an error in parallelism. All rotating components have a beam deviation of less than 1 arcmin. During the project, we noticed that previous components with a beam deviation of less than 20 arcmin, would cause the laser spot to rotate while the optical component was rotating. This resulted in an incorrect measurement as different spot on the sample would be analyzed across a full range of rotation.

This issue was discovered when rotating the optical components by 180 degrees and seeing a Raman spectra with noticeably different intensities for the Raman active modes. Photos were taken of the sample and the beam when the optical component at 0 degrees rotation and at 180 degrees rotation using hte 100x Objective lens. Afterwards, the locations of the beams are noted and the distance between them is calculated. The issue was resolved upon the mounting of higher quality optics with a lower error in parallelism. Repeating the previous method of detecting beam deviation results in no noticeable change in beam location.

# 4 Results and discussion

## 4.1 Thickness

Since the intensity and degradation rate of the Raman modes is dependent on the thickness of BP, it is necessary to note the thickness of the flake being examined.

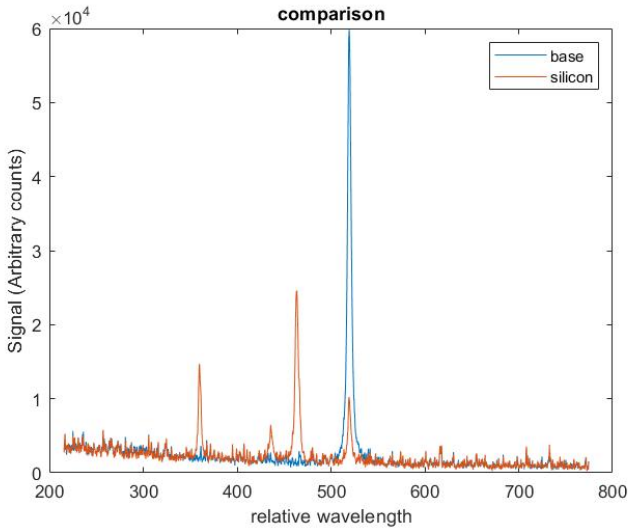


Figure 12: Silicon underneath BP vs Silicon signal

The thickness for the BP flake is estimated by using the absorption coefficient from [30] and the Beer-Lambert law to derive an estimator for the thickness of the BP flake:

$$d = \frac{log(T)}{2\alpha_{BP}} \tag{44}$$

where d is the estimated thickness of the BP, T, is the ratio of the signal strength of the silicon substrate and the silicon beneath the BP and $\alpha_{BP}$ is the absorption coefficent of BP. From equation 44, the estimated thickness is 88 nm. This thickness is likely overestimated because the laser used by Li *et al.* is of a shorter wavelength (520 nm) than the one used in this experiment.

## 4.2 Comparison with theory and other experiments

Data from the Raman microscope was acquired in order to measure the intensity of the 3 Raman-active phonon modes. Figure 13 shows the raw data of multiple Raman spectra of BP at different polarization settings. Raman peaks can be seen around 357 $cm^{-1}$, 435 $cm^{-1}$ and 463 $cm^{-1}$. As discussed in section 2.3, these are the $A_g^1$, $B_{2g}$ and $A_g^2$ modes respectively. By rotating the optical components as explained in the methods section, one can manipulate the active and detectable phonon modes through the incoming polarized light.

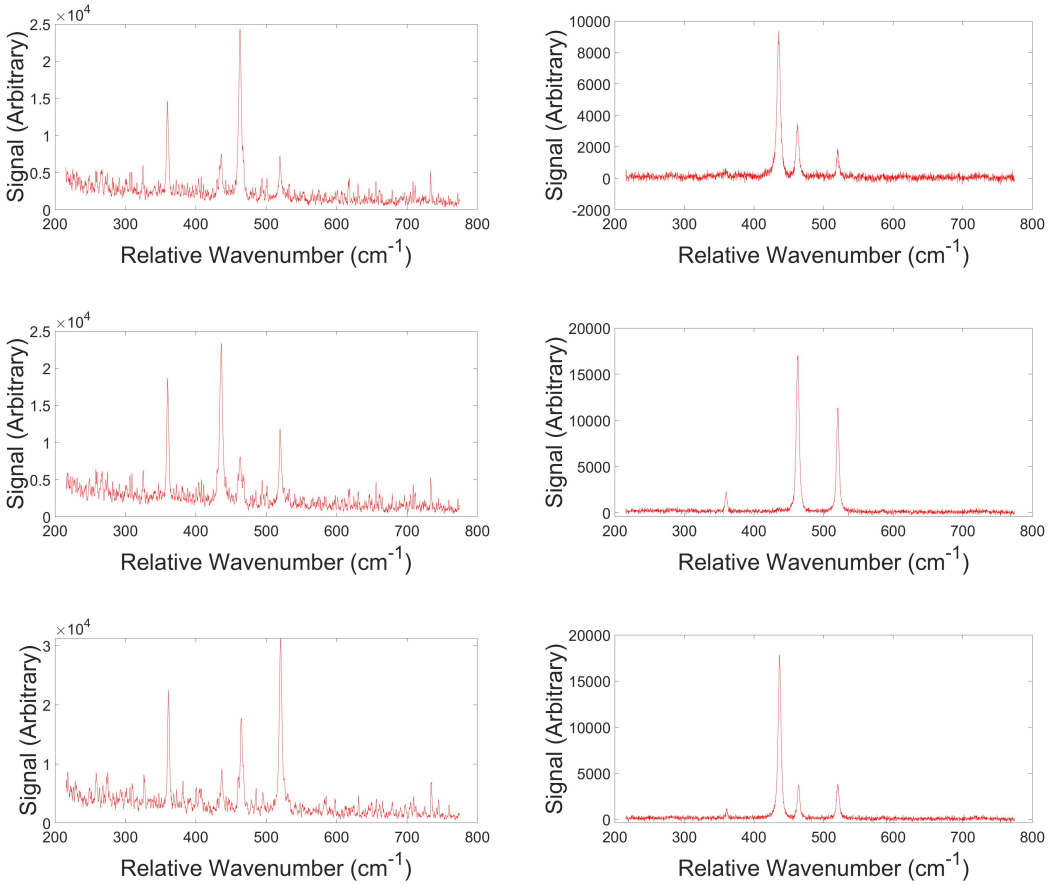


Figure 13: Some Raman spectra of BP at different polarizations. Parallel configuration(left). Cross configuration(right)

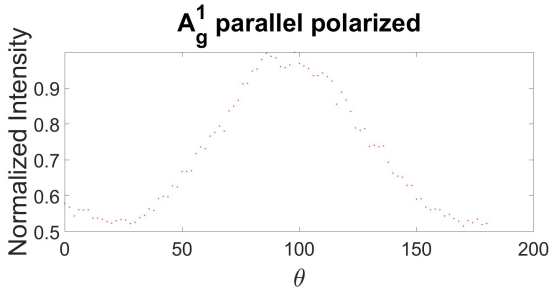


(a) $A_g^1$ mode peak intensity plotted against angle (parallel)

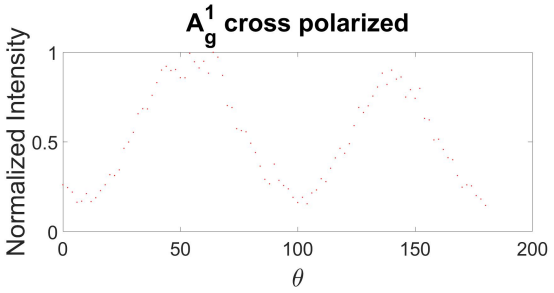


(b) $A_g^1$ mode peak intensity plotted against angle (cross)

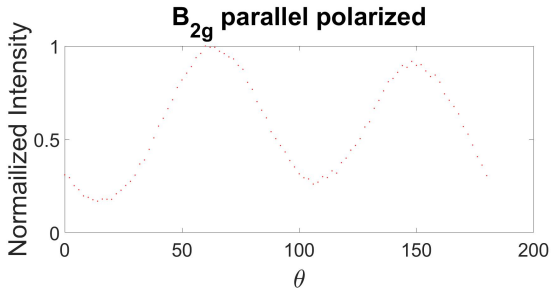


(c) $B_{2g}$ mode peak intensity plotted against angle (parallel)

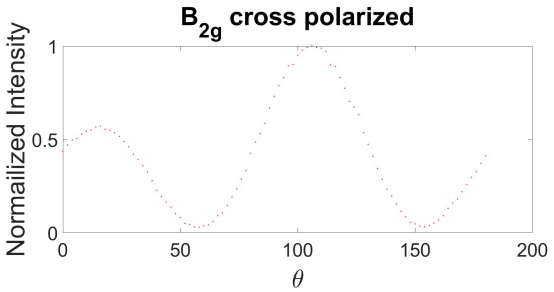


(d) $B_{2g}$ mode peak intensity plotted against angle (cross)

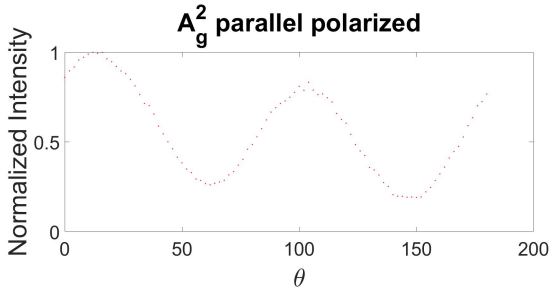


(e) $A_g^1$ mode peak intensity plotted against angle (parallel)

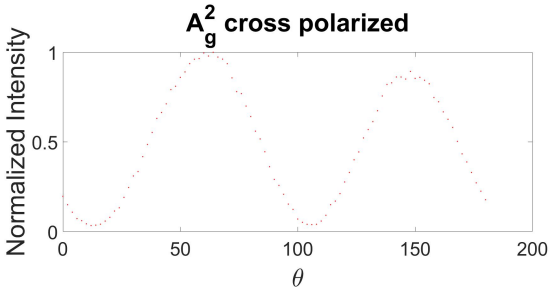


(f) $A_g^1$ mode peak intensity plotted against angle (cross)

Figure 14: Raw data. Parallel setup(left). Cross setup(right)

The peak intensity of the different modes were extracted from the Raman spectra in order to determine their angular dependence. The graphs in figure 14 are the peaks of the respective modes plotted against the angle that the incoming laser light polarization has been rotated. The data has been normalized to the highest peak intensity of the mode e.g. all data associated with the $A_g^1$ mode is normalized by the highest $A_g^1$ peak intensity detected.

As suggested by theory, the intensity of the different Raman modes follow a periodic pattern of sinusoidal functions. These functions partly follow the proposed theory, but as brought up from [28], the basic theory for the quantitative analysis of the angular dependence of the Raman mode intensities are inadequate for all settings.

Figures 15a, 15b and 15c are the parallel configurations fitted to the equations in section 2.8. Figures 15a and 15care are fitted to equation 25, while figure 15b is fitted to 27. The data in the parallel configuration well fit the theory presented.

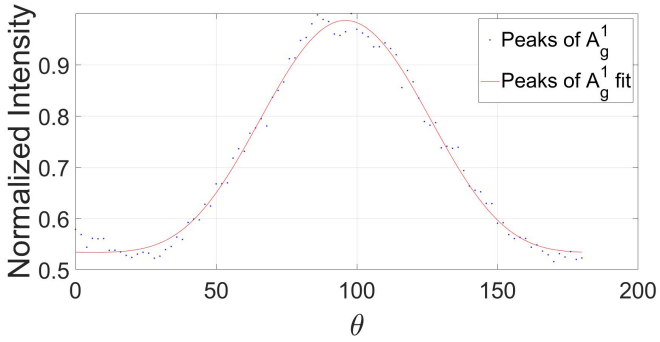


(a) $A_g^1$ fitted parallel

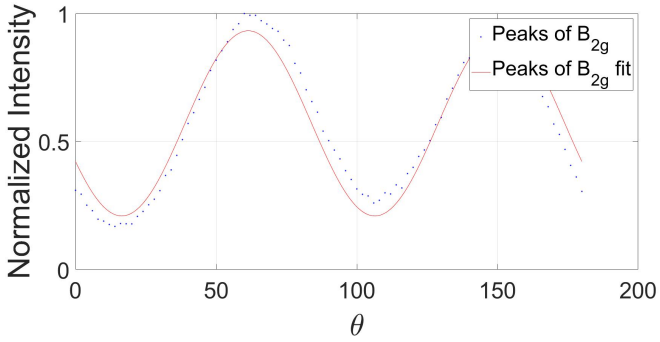


(b) $B_{2g}$ fitted parallel

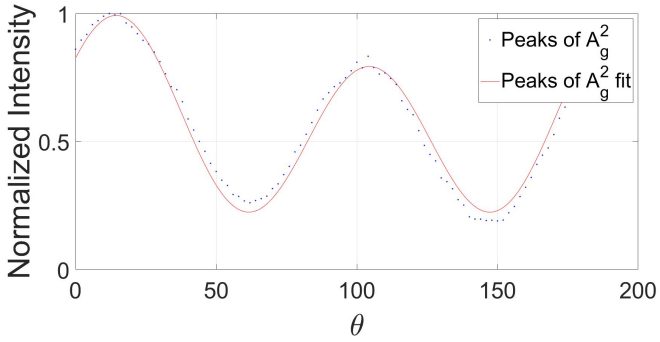


(c) $A_g^2$ fitted parallel

Figure 15: Fitted parallel configuration

Since the equations are general equations, the phase of the angular intensity must be matched to the data. In addition to deriving the Raman tensor parameters from the fit, the phase of the data had to be matched with the theory. The period of the angular

dependence of BP is 180 degrees and an additional shift is added to the period to account for the fact that the incident polarization of light may not match the orientation of the BP.

Figures 16a, 16b, 16c show the cross polarized setup fitted to equations 26 for the $A_g$ modes and 28 for the $B_{2g}$ mode. The non-zero Raman components are taken from the fits made in the parallel configuration. Despite having strong correlation with the parallel configuration, the predicted angular dependency of the Raman peaks has major discrepancies with the data. The $A_g^1$ and $B_{2g}$ modes fit follows the period but does not perfectly model the peaks while the $A_g^2$ mode fit completely fails to emulate the data.

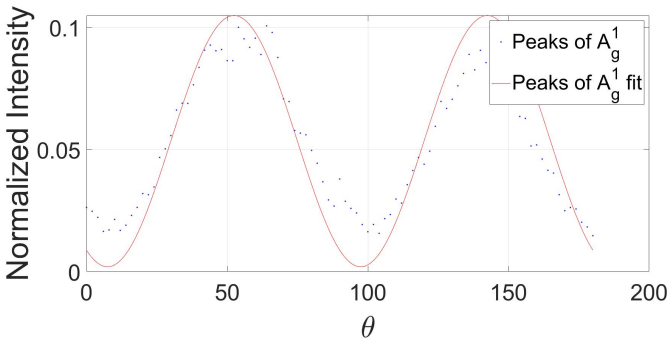


(a) $A_g^1$ fitted cross

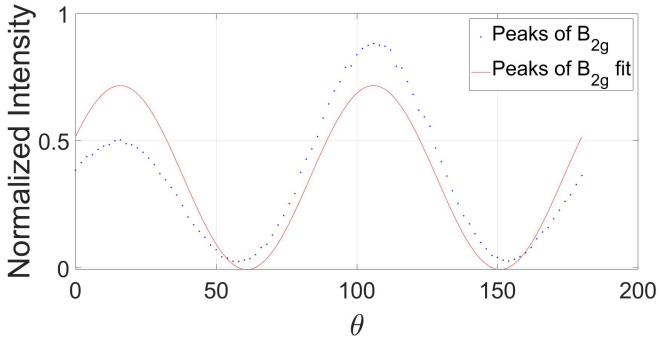


(b) $B_{2g}$ fitted cross

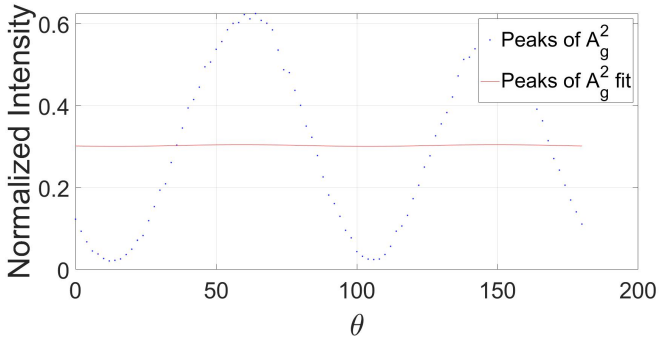


(c) $A_g^2$ fitted cross

Figure 16: Fitted cross configuration

A solution to this problem was proposed by Ribeiro *et al.* in [28]. The article proposed that the discrepancy between the predicted angular dependence and the actual angular dependence was due to the linear dichroism in BP. To correct the theory, it was suggested to account for light absorption in the Raman tensor. Table 1 shows the values derived from the new fits.

Table 1: Mode and additional phase values

| Mode | a | c | $\phi_{ca}$ |
|---|---|---|---|
| $A_g^1$ | 0.5997 | 0.2265 | 67 |
| $A_g^2$ | 0.8884 | 1.004 | 151.4 |

Table 1 has the non-zero Raman tensor elements, a and c, of the $A_g$ modes and the $\phi_{ca}$. All values in the table were derived from the new enhanced fits applied to the data from the parallel configuration.

The $A_g^1$ mode has a greater a parameter which shows that the xx component of the dielectric constant modulates the $A_g^1$ mode more than the zz component. This is inconsistent with what was reported in [28].On the other hand, the $A_g^2$ mode has a greater c parameter which shows the opposite to be the case for that particular mode. This is consistent with what was reported in [28].

The Raman tensor phase, $\phi_{ca}$ has a non-zero value for the $A_g^1$ mode that is inconsistent with [28] while the $\phi_{ca}$ for the fit from the $A_g^2$ is greater than that from the fit of the $A_g^1$ mode, which is consistent with [28]

Table 2 shows the different goodness of fits from the older models based on the textbook theory and the new model proposed by Ribeiro [28].

Table 2: Mode and additional phase values

| Mode | RMSE textbook model | RMSE model with phase |
|---|---|---|
| $A_g^1$parallel | 0.0174 | 0.0173 |
| $A_g^2$parallel | 0.0414 | 0.0182 |
| $A_g^1$cross | 0.0136 | 0.0083 |
| $A_g^2$cross | 0.2013 | 0.1063 |

Overall, the enhanced fits for the parallel configuration show minor improvement as seen in Figure 17b and 17d. The fit for the $A_g^1$ mode shows little change, while the fit for the $A_g^2$ mode shows a minor improvement.

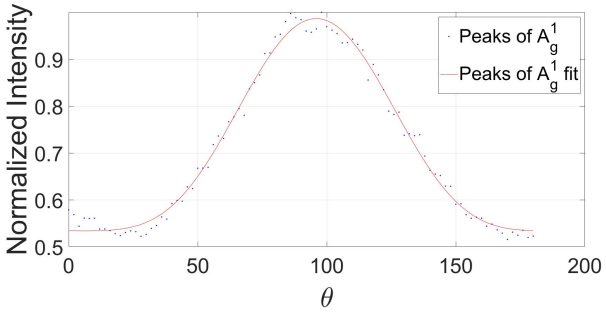


(a) $A_g^1$ parallel

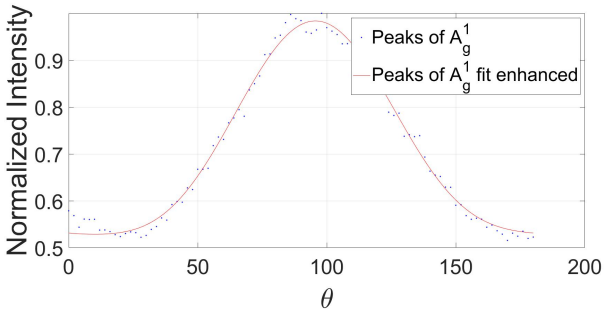


(b) $A_g^1$ parallel with phase

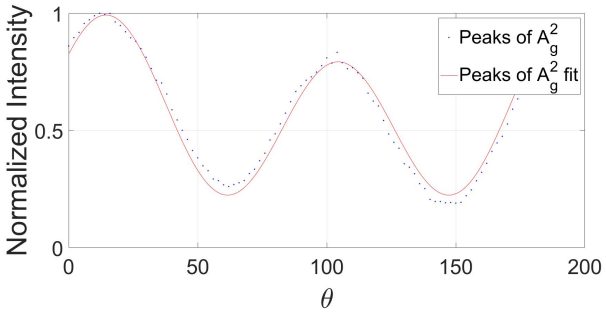


(c) $A_g^2$ Parallel

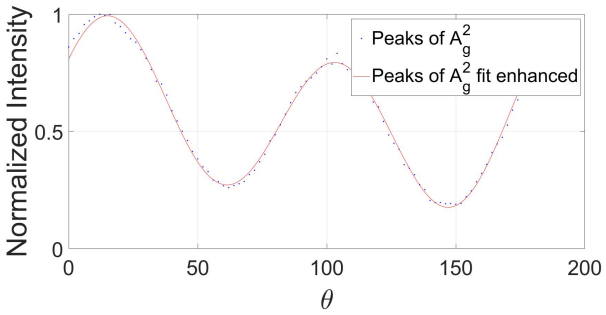


(d) $A_g^2$ parallel with phase

Figure 17: Model with additional phase (parallel)

Using the values seen in table 1, new enhanced fits were generated for the cross polarized configuration as seen in figures 18b and 18d. The improvement in fit is in agreement with [28], however, there were some discrepancies between the two experiments. The first discrepancy is with the $A_g^1$ mode. Unlike the results found in [28], the $A_g^1$ mode in the cross polarized setting does not match the standard Raman tensor formula given earlier, however this is solved with the addition of the Raman tensor phase. The next discrepancy is the $B_{2g}$ mode in the cross polarized position. Equation 39 is effectively the same as 28, and therefore no change was observed. Finally, despite the drastic improvement in the fit between the data and the model, the $A_g^2$ mode still overshoots the data at the peaks and the troughs. This may be from an additional dependence on the thickness of the sample that is not accounted for in theory.

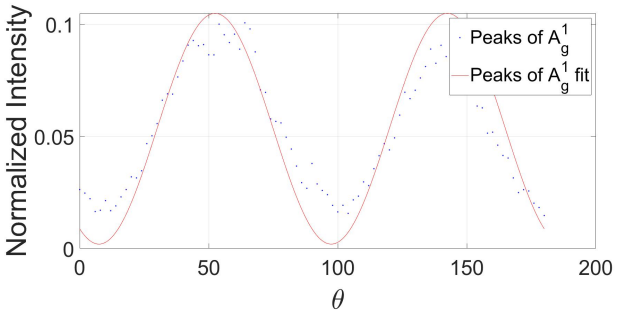


(a) $A_g^1$ cross

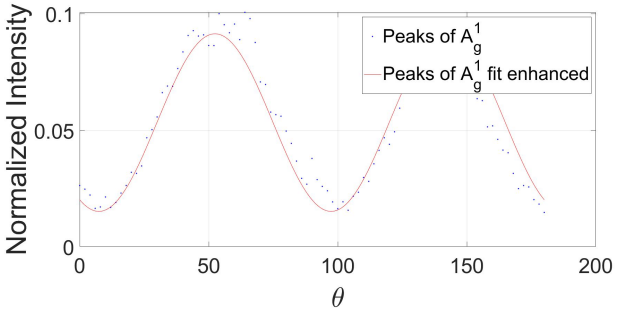


(b) $A_g^2$ cross with phase

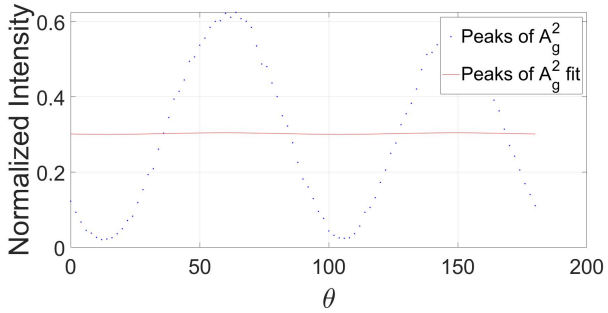


(c) $A_g^2$ cross

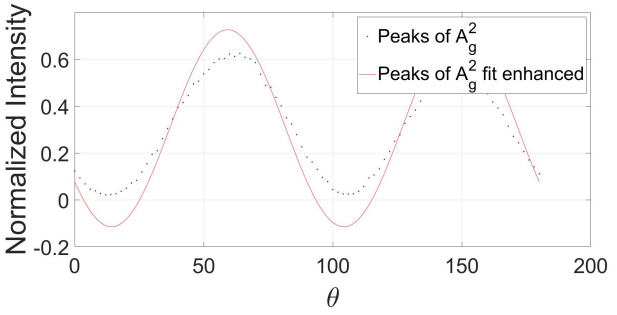


(d) $A_g^2$ cross with phase

Figure 18: Model with additional phase (cross)

## 4.3 Degradation

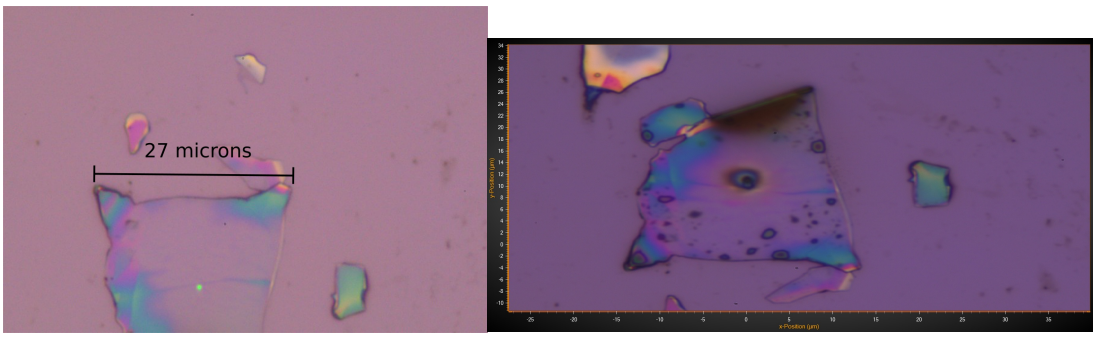


(a) Photo of sample before extended exposure

(b) Photo of sample after extended exposure

Figure 19: BP Before and after pictures of of long exposure to light

To determine what effect the degradation might have on the BP sample, constant exposure recording session was initialized after the the main phonon mode control was completed. The polarization of the incident light was fixed and set to the parallel polarized configuration.

Figure 19 shows the BP sample before and after the constant recording session. After the 11.5 hours of constant exposure was completed, visible dark markings can be seen on the BP flake with the largest of the dark spots located where the beam was at the center of the flake in figure 19b. Surrounding the dark marks are interference fringes. These interference have been reported to be caused by trace liquids such as water of phosphoric acid on the surface of BP [21]. These bubbles form over degraded areas and cause oscillations in the Raman intensity.

Across all the data, there is a consistent drop in signal strength in the later angles. Theoretically, the initial signal at 0 degrees should be identical with the angle at 180 degrees. Across all the measured modes, there are differences between the model and the experimental data. For example, in the enhanced $A_g^1$ cross fit, the model under predicts the signal from 0 degrees to 90 degrees but over predicts the signal from 90 to 180 degrees.

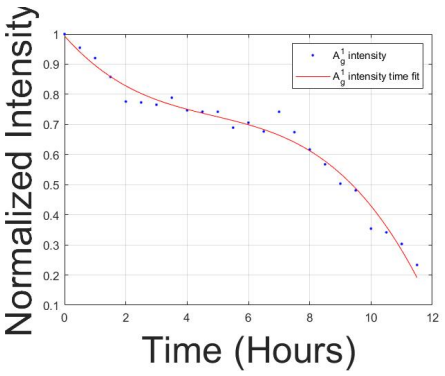


(a) $A_g^1$ parallel in time

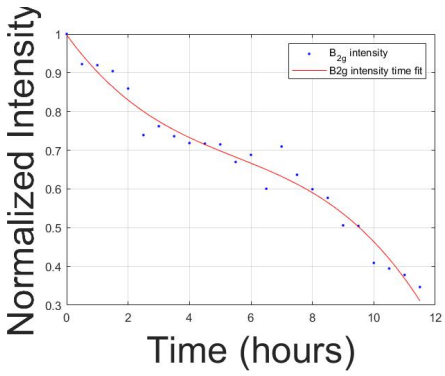


(b) $B_{2g}$ parallel in time

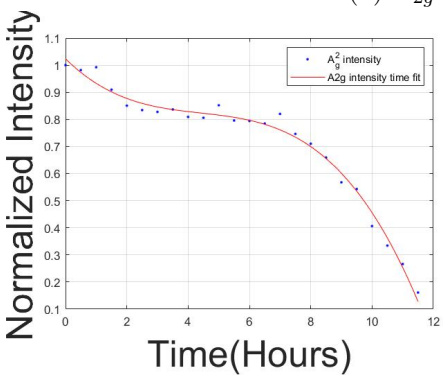


(c) $A_g^2$ parallel in time

Figure 20: Decay of intensity for all the modes over time

Figures 20a, 20b, 20c show the Raman spectra of BP over 11.5 hours of constant exposure. It can be seen that the intensity of the Raman active modes have degraded almost completely by 11.5 hours. All modes suffer from a major decline in intensity. One can model the decline in signal between all the modes to approximate the rate of degradation. A 3rd degree polynomial fit seemed to properly follow the rate of degradation for all the modes as can be seen in the figures. The intensity of the modes fail to demonstrate the increase in intensity measured in [22], however this may be due to constant exposure to the 532 nm laser light.

It is assumed that each dataset took 40 minutes to complete, and each datapoint took the same amount of time to take. This rate is substituted into the 3rd order polynomial fit and used to renormalize the dataset. The result is figure 21. The enhanced fits retain the same goodness of fit while the data looks more consistent with theory as the 0 and 180 degree data points are much closer to each other's value with the exception of figure 21c, where the intensity value at 180 degrees is still much higher than the intensity value at 0 degrees.

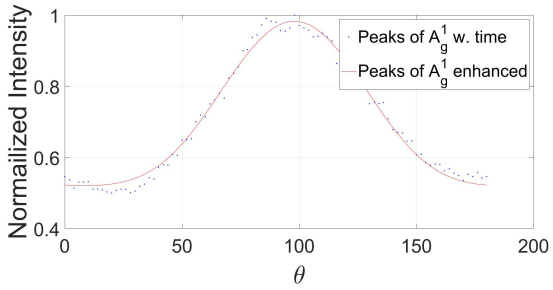


(a) $A_g^1$ enhanced fit with time consideration (parallel)

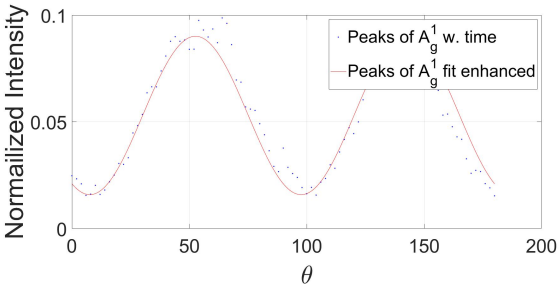


(b) $A_g^1$ enhanced fit with time consideration (cross)

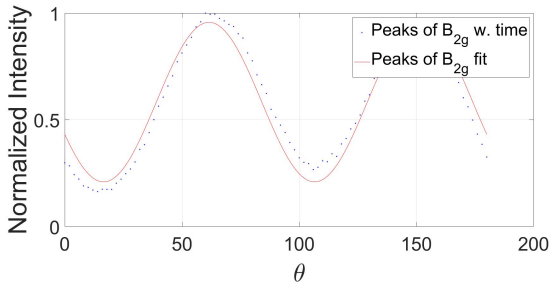


(c) $B_{2g}$ enhanced fit with time consideration (parallel)

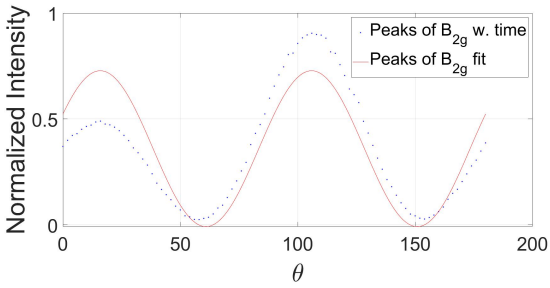


(d) $B_{2g}$ enhanced fit with time consideration (cross)

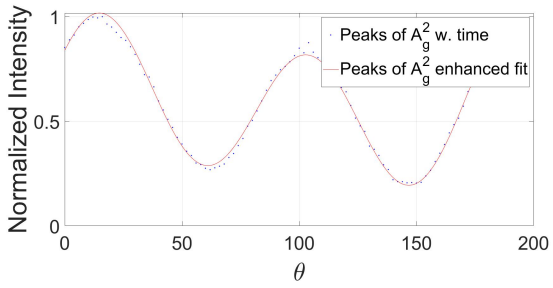


(e) $A_g^2$ enhanced fit with time consideration (parallel)

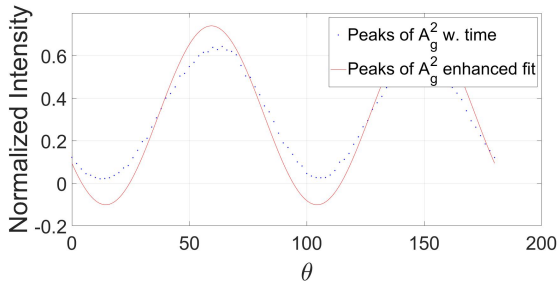


(f) $A_g^2$ enhanced fit with time consideration (cross)

Figure 21: data with time taken into account and refitted with the enhanced fit

# 5 Conclusion

This Master's project presents the results from an experiment aiming to control the phonon modes of BP through polarized Raman excitation. The phonon modes were modulated by manipulating the polarization of the incident light with a half-wave plate and polarizer. The intensity of the phonon modes followed an angular dependence that needed to include the complex variables of absorptive material to properly account for the phase, however the fits were still not precise as some modes such as the $A_g^2$ mode in the cross polarized position where overestimated at the peaks and troughs. The BP was prepared in the standard method of mechanical exfoliation and considerations were taken to account for the degradation of BP and the thickness of the flake. Phonon mode control closely follows the theory but additional factors such as degradation and thickness affect the modes in ways that the current theory does not fully account for.

# 6 Outlook

Due to the relatively unstudied nature of BP, there are many potential experiments that can be pursued to further understand the material or improvements that can be made to the current experiment to increase precision, Based off of this experiment, further efforts can be put into:

1. **Better equipment when undertaking Phonon mode control:** As can be seen in the results of this project, the expression for angular dependence of BP does not perfectly suit the data, therefore it can be beneficial to perform the experiment with more automated tools to keep things such as the rate of rotation of the optical components more constant.

2. **Enhanced BP preservation techniques:** Because BP signal suffers from degradation, it can be beneficial to coat BP with a substance such as a passivation layer to slow down degradation whilst the experiment is being performed.

3. **Further research into the effects of degradation:** Alternatively, more research could be done with the degradation as the primary focus. Different factors such as laser frequency and polarization can be altered to test if such characteristics may alter the rate of degradation.

# 7 References


[1] Rui Gusmao, Zdenek Soferm and Martin Pumera .Black Phosphorus Rediscovered: From Bulk Material to Monolayers. *Angewandte International edition Chemie* 56(28): 8052-8072. 2017.

[2] Low *et al.* Tunable optical properties of multilayer black phosphorus thin films. *Phys. Rev. B* 90(7): 075434. 2014

[3] Chaves A. Theoretical Overview of Black Phosphorus. *Cambridge University Press* 3(21):381-412. 2017.

[4] C. A. Vanderborgh and D. Schiferl. Raman studies of black phosphorus from 0.25 to 7.7 GPa at 15 K. *Phys. Rev. B* 40: 9595. 1989.

[5] Guo *et al.*From Black Phosphorus to Phosphorene: Basic Solvent Exfoliation, Evolution of Raman Scattering, and Applications to Ultrafast Photonics. *Advanced Functional Materials* 25(45): 6996-7002. 2015.

[6] A Favron *et al.* Photooxidation and quantum confinement effects in exfoliated black phosphorus *Nature materials* 14(8): 826. 2014.

[7] A. Mohammed. Theoretical Studies of Raman Scattering. KTH. 2011.

[8] Stacy Liang, Md Nazmul Hasan and Jung-Hun Seo. Direct Observation of Raman Spectra in Black Phosphorus under Uniaxial Strain Conditions.*Nanomaterials* 9: 566. 2019.

[9] Lu *et al.*. Probing the anisotropic behaviours of black phosphorus by transmission electron microscope, angular dependent Raman spectra and electronic transports measurements. *Applied Physics Letters* 107(2):215-224. 2015.

[10] Henrique B. Ribeiro, Marcos A. Pimenta and Christiano J.S. de Matos. Raman spectroscopy in black phosphorus. *Journal of Raman spectroscopy* 49(1): 76-90. 2018.

[11] M. Baibarac, A. Nila, I Baltog. Polarized Raman Spectra of phosphorene in edge and top view measuring configurations. *RSC Adv.* 6:58003. 2016.

[12] Kim *et al.* Anomalous polarization dependence of Raman scattering and crystallographic orientation of black phosphorus. *Nanoscale* 7: 18708-18715. 2015.

[13] Laurence Nafie, *et al.* Angular Dependence of Raman Scattering Intensity.*The Journal of Chemical Physics* 52:1584. 1970.

[14] Juanxia Wu et al. Identifying the Crystalline Orientation of Black Phosphorus Using Angle-Resolved Polarized Raman Spectroscopy. *Angewandte Chem Int. Ed.* 54: 2366-2369. 2015.

[15] Jenaina Ribeiro Soares. Group Theory and Raman Spectroscopy applied to the study

of Two-Dimensional Materials. Universidade Federal de Lavras. 2014.

[16] Lucjan Piela. *Ideas of Quantum Chemistry Appendix C: Group theory and Spectroscopy.* Elsevier BV. 2003.

[17] A.Zee. *Group Theory in a Nutshell for Physicists.* Princeton University Press. 2016

[18] M.S. Dresselhaus. G. Dresselhaus and A. Jorio. *Group Theory - Application to the Physics of Condensed Matter.* Berlin-Heidelberg: Springer-Verlag, 2008.

[19] C Kittel. *Introduction to Solid State Physics.* Wiley, 2004.

[20] P. W. Atkins, M. S. Child, and C. S. G. Philipps. *Tables for Group Theory.* Oxford University Press, 2006.

[21] Fadhel Alsaffar *et al.* Raman Sensitive Degradation and Etching Dynamics of Exfoliated Black Phosphorus. *Nature* 7:44540. 2017.

[22] Sruthi Kuriakose *et al.*Black Phosphorus: ambient degradation and strategies for protection. *2D Materials* 5:032001. 2018

[23] Jackson, John D. *Classical Electrodynamics (3rd ed.).* New York: John Wiley Sons, 1998.

[24] E. Collett. *Field Guide to Polarization.* Bellingham:SPIE Press, 2005.

[25] V. Elena. Light propagation in an anisotropically scattering medium. KTH.2018.

[26] J. Toporski,T. Dieing. *Confocal Raman Microscopy Second Edition.* Cham: Springer, 2018.

[27] Saleh, B.E.A. Teich, M.C. *Fundamentals of Photonics Chapter 6 - Polarization Optics.* Wiley, 2007.

[28] Henrico Ribeiro *et al.* Unusual Angular dependence of Raman of the Raman response in Black Phosphorus.*ACS Nano* 9(4): 4270-4276. 2015.

[29] Eric Nilsson. Ultrafast Transient coherent Raman Microscopy (TRam). Lund University. 2019.

[30] Diao Li *et al.* Polarization and Thickness Dependent Absorption Properties of Black Phosphorus: New Saturable Absorber for Ultrafast Pulse Generation. *Nature Scientific Reports* 5:15899. 2015.

[31] Gao *et al.* Mechanical exfoliation of two-dimensional materials. *Journal of the Mechanics and Physics of Solids* 115: 248-262. 2018.

[32] Safety Data Sheet – Black Phosphorus v1.3. *ACS Material LLC.* 2016.

# 8 Sample preparation

## 8.1 Materials

1. BP purchased from hq Graphene
2. Latex gloves
3. tweezers
4. European Standard EN 149 mask
5. European standard EN166 eyewear
6. Micronova™ CR100 PC™ Cleanroom Tape [5]
7. 3.5 cm diameter silicon substrate
8. Flat tweezers
9. Fumehood in room

[5] Although the process can be achieved with scotch tape, the 'blue tape' used in this procedure has a weaker adhesive, is easier to peel with and leaves less residue on the sample when finished.

## 8.2 Process

The sample was prepared via mechanical exfoliation [31]. This involves using tape to mechanically remove layers off of a 2D layered material to deposit onto a substrate. An idealized situation can be seen in figure 22. Gao *et al.* [31] provides an in depth discussion on the physics of mechanical exfoliation however much of the mathematics behind the physics is difficult to achieve in reality due to human error. Perfectly peeling a 2D sheet onto a substrate on the first iteration is unlikely and often requires multiple trials to peel off thinner layers.

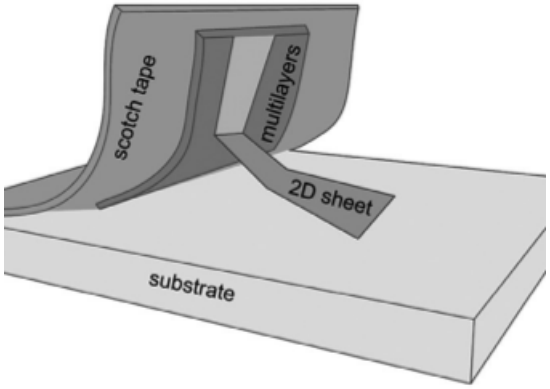


Figure 22: Ideal Mechanical exfoliation situation [31]

Since the health hazard effects of BP are still relatively unknown [32], additional precautions were taken to prevent possible injury or irritation. The BP was peeled underneath a fume hood to prevent inhalation and unwanted environmental scattering. Gloves were worn during peeling to prevent contact with skin. Graphene was used in place of BP for clearer pictures and to prevent any unnecessary degradation to the BP. The process is mostly identical with the exception that graphene peeling does not require a fume hood and mask.

The steps:

1. Lay out a clean section such as an aluminum foil base to rest all the items and the sample

2. Prepare multiple strips of tape

3. Take tape with tweezer and place the unused section onto sample

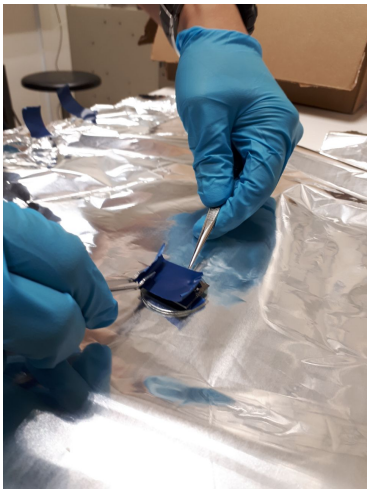

4. Remove tape from sample slowly at about a 120 degree angle.

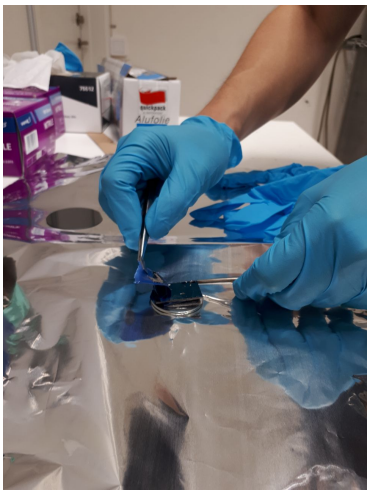

5. Place tape with material onto fresh tape

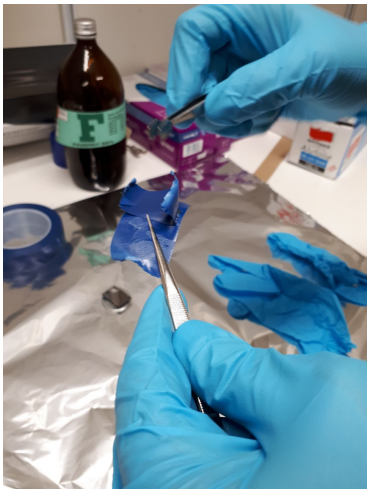

6. Separate tape from each other and repeat the step 5 and 6 eight more times with fresh tape

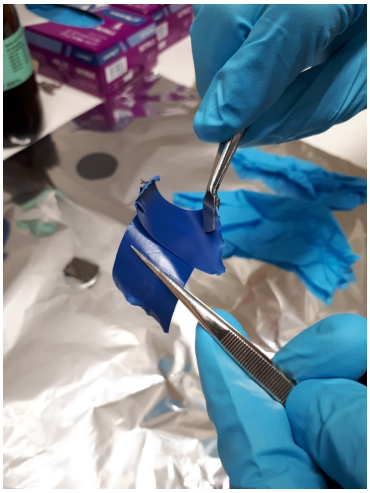

7. With the last piece of tape place the tape on the silicon substrate


8. Finally, peel the tape off the silicon in a manner similar to how the tape was peeled off the sample

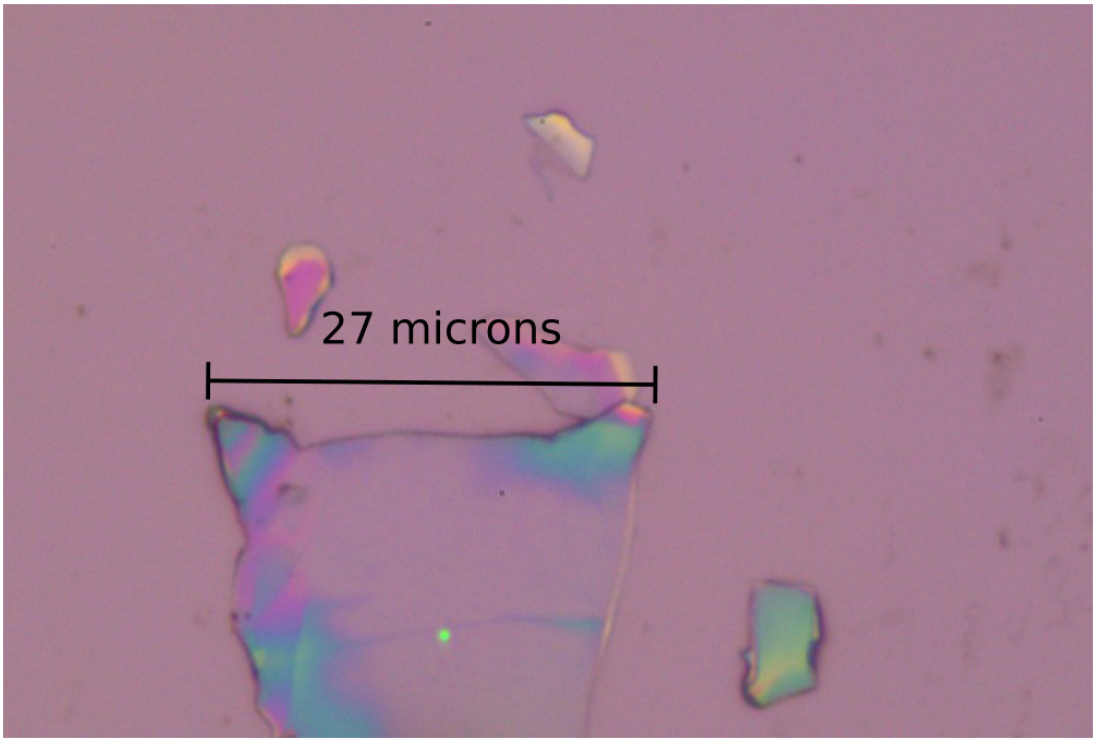


Figure 23: A BP flake underneath a 100x objective microscope

After the tape is removed and the sample is deposited on the silicon substrate, the substrate is placed underneath an optical microscope to determine if the preparation was a success. A grid system is established where a unique point on the substrate is designated as (0,0). In this case, the lower right edge of the substrate was used.

The expected deposit site of the sample is then checked with an optical microscope and any interesting flakes seen under such in figure 23 are noted on the grid system before changing to a more powerful objective lens for analysis.